Cryo-electron Microscopy Imaging of Alzheimer's Amyloid-beta 42 Oligomer Displayed on a Functionally and Structurally Relevant Scaffold

Jinming Wu, Thorsten B. Blum, Daniel P Farrell, Frank DiMaio, Jan Pieter Abrahams, and Jinghui Luo*

Abstract: Amyloid-β peptide (Aβ) oligomers are pathogenic species of amyloid aggregates in Alzheimer's disease. Like certain protein toxins, Aβ oligomers permeabilize cellular membranes, presumably through a pore formation mechanism. Owing to their structural and stoichiometric heterogeneity, the structure of these pores remains to be characterized. We studied a functional Aβ42-pore equivalent, created by fusing Aβ42 to the oligomerizing, soluble domain of the α-hemolysin (αHL) toxin. Our data reveal Aβ42-αHL oligomers to share major structural, functional, and biological properties with wild-type Aβ42-pores. Single-particle cryo-EM analysis of Aβ42-αHL oligomers (with an overall 3.3 Å resolution) reveals the Aβ42-pore region to be intrinsically flexible. The Aβ42-αHL oligomers will allow many of the features of the wild-type amyloid oligomers to be studied that cannot be otherwise, and may be a highly specific antigen for the development of immuno-base diagnostics and therapies.

Introduction

Alzheimer's disease (AD) is characterized by Aβ plaques and tau neurofibrillary tangles (NFTs) deposited in the brains of the patients and stepwise dementia.[1] Aβ is a peptide, cleaved from intramembrane proteolytic processing of amyloid precursor protein (APP) by β-/γ-secretase.[2] The Aβ peptides aggregate into soluble oligomers, protofibrils, and eventually deposit as insoluble fibrils. Among these aggregates, Aβ oligomers are the most toxic species, responsible for neuronal dysfunction. Like certain protein neuro- and hemolytic toxins, Aβ oligomers are presumed to elicit pore formation in cellular membranes, which may cause local depolarization or other cellular dysfunctions. It has been observed by electron microscopy that the Aβ40 mutant (E22G) forms pore-like structure,[3] and that Aβ oligomers display ion-channel activity in lipid membranes with a range of conductances.[4] The oligomeric Aβ channel activity has been also confirmed in *Xenopus laevis* oocytes by single-channel Ca^{2+} imaging.[5] Nuclear magnetic resonance (NMR) and single-channel electrical recordings further revealed that micelle-stabilized Aβ42 oligomers insert as β-barrel pores into lipid membranes with different conductances.[6] In addition, Aβ oligomers may permeabilize membranes with non-specific pore formation.[7] These observations indicate the importance of a lipidic environment for the characterization, stabilization and toxicity of Aβ oligomers. Also, the channel conductance discrepancy among the different studies may be caused by their transient nature, structural and stoichiometric heterogeneity.[8] So far, stoichiometry-defined and stable Aβ oligomers remain to be explored in a lipidic environment, as these are potentially valuable for determining the structure and developing conformation-specific antibodies.

To stabilize and display Aβ42 oligomers in a membrane environment for structure determination, we designed a α-hemolysin (αHL) scaffold. Secreted by *S.aureus*, αHL can assemble into a lipid-soluble, heptameric toxin, with a transmembrane β-barrel and an outer membrane domain.[9] The transmembrane β-barrel structure of the αHL oligomer is reminiscent of the proposed β-barrel-type structure of Aβ42 oligomers in detergent micelles.[6b] We speculated that the soluble, heptamer-inducing domain of αHL might structurally induce the Aβ42 peptides to adopt a well-defined oligomeric state with enhanced size and symmetry, thus providing a good model system for determining its functional properties and structure by biophysical methods, including single-particle cryo-EM imaging. This idea was inspired by reports that wild-type (WT) αHL shares structural and functional homology with Aβ42 oligomers.[10] We hypothesized that WT αHL and WT Aβ oligomers might share similar mechanisms of membrane permeabilization, and that both the β-hairpins in the β-barrel of αHL and Aβ oligomers interact with lipid membranes in a similar manner. To investigate whether αHL could offer a functionally relevant scaffold for oligomerizing

[*] J. Wu, Dr. T. B. Blum, Prof. Dr. J. P. Abrahams, Dr. J. Luo
Department of Biology and Chemistry, Paul Scherrer Institute
5232 Villigen (Switzerland)
E-mail: Jinghui.luo@psi.ch

D. P Farrell, Dr. F. DiMaio
Department of Biochemistry, University of Washington
Seattle, WA 98195 (USA)
and
Institute for Protein Design, University of Washington
Seattle, WA 98195 (USA)

Prof. Dr. J. P. Abrahams
Biozentrum, University of Basel
4058 Basel (Switzerland)

Supporting information and the ORCID identification number(s) for the author(s) of this article can be found under:
https://doi.org/10.1002/anie.202104497.
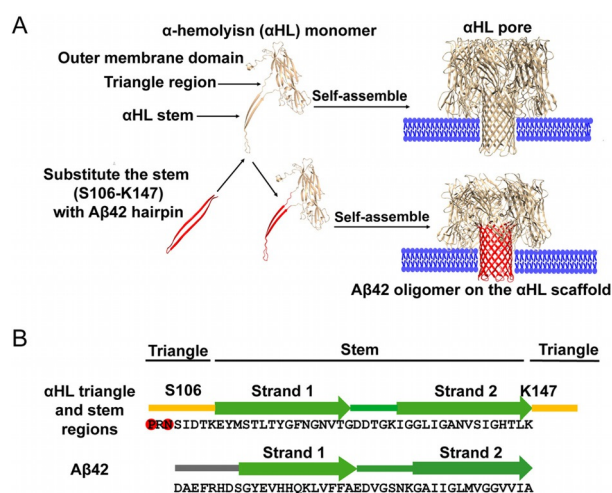
Figure 1. A) The Aβ42 sequence (red) fused to the soluble domain of α-hemolysin (αHL; yellow) forms a heptameric pore complex that can insert into lipid membranes (blue). B) Sequence comparison of the triangle and stem regions from WT αHL and Aβ42. The sequences were aligned based on the secondary structure elements from the αHL crystal structure (PDB: 7AHL) and the Aβ hairpin NMR structure (PDB: 2OTK and 2BEG). The stem hairpin is surrounded by two triangle sequences (in yellow) from αHL including the Y102-K110 and Y148-D152 residues,[9] that include two residues (P103 and N105; in red) that are important for the assembly of the hairpins.[11] The stem is composed of two antiparallel β strands (strand 1, E101-K126 residues and strand 2, I132-K147). In the complex of affibody and Aβ40[12] or Aβ42 fibril,[13] Aβ residues K16-A42 form a β-hairpin, while the structure of the other parts remain to be determined.

and displaying Aβ42 oligomers for structure determination, we replaced the transmembrane β-hairpin of αHL with an Aβ42 sequence (Figure 1). Here, we show that the Aβ sequence is required for oligomerization. A hemolytic assay, single-channel electrical recordings, western blot and cell viability assays confirmed that the displayed oligomers are functionally and toxicologically relevant to the wild type, allowing us to determine the structure of the oligomer by single-particle cryo-EM.

Results and Discussion

The transmembrane β-barrel of heptameric αHL consists of seven β-hairpins, formed by residues Y110-K147.[9] Like monomeric Aβ42, the region of residues Y110-K147 is flexible in the monomeric state. Also, it forms a stable hairpin structure in the oligomeric state.[14] The oligomerization of αHL may be influenced by the triangle region (residues Y102-K110 and Y148-D152 shown in Figure 1B). For instance, the mutations P103C and N105C can compromise the assembly of αHL.[11] The stem residues Y110-K147 are similar to the hairpin structure of Aβ in the presence of affibody or in fibrils, as determined by NMR,[12,13] whilst the structure of the N-terminus of Aβ42 remains unclear. To display and oligomerize Aβ42 on the scaffold, we kept residues P103 and N105 in the triangle region and substituted the residues starting from S106, with the Aβ42 residues.

In a membrane environment, the β-hairpin sequence (D106-K147) of monomeric WT αHL oligomerizes into heptameric pores. In our study, we substituted the β-hairpin sequence of αHL with an amyloid sequence, Aβ42, Aβ11-42, Aβ1-28, Aβ1-17, Aβ0, or hIAPP (human islet amyloid polypeptide that is associated with type 2 diabetes[15]; Supporting Information, Figure S1). We purified these His-tagged αHL constructs in the presence of 0.38 mM DDM micelles using Co-NTA chromatography and verified them by LC-MS (Figure S2). The Aβ42-αHL, Aβ11-42-αHL, hIAPP-αHL or WT αHL proteins form heptamers but the other constructs migrate as monomers on SDS-PAGE (Figure 2 A). Displayed on the same αHL scaffold, the Aβ42 and hIAPP complexes sequences differ in their electrophoretic mobility, where the hIAPP-αHL hybrid complex appears to have a lower molecular weight, presumably forming a water-filled trimeric β-sandwich confirmed by molecular dynamics simulation.[16] Co-NTA chromatography imidazole gradient fractionation eluted oligomers and monomers separately from the column (Figure S3). The hybrid Aβ1-28 and Aβ1-17 sequences do not oligomerize even at the highest concentration of imidazole (250 mM). This is consistent with the observation that Aβ1-17 or Aβ1-28 alone cannot form oligomers in lipid membranes.[17] The oligomerization requires the presence of Aβ sequences, since upon Aβ42 deletion, (Aβ0, Figure 2 A, line 7), the αHL scaffold remains monomeric. We investigated the surface hydrophobic reorganization of these oligomers by 8-anilino-1-naphthalenesulfonic acid (ANS)
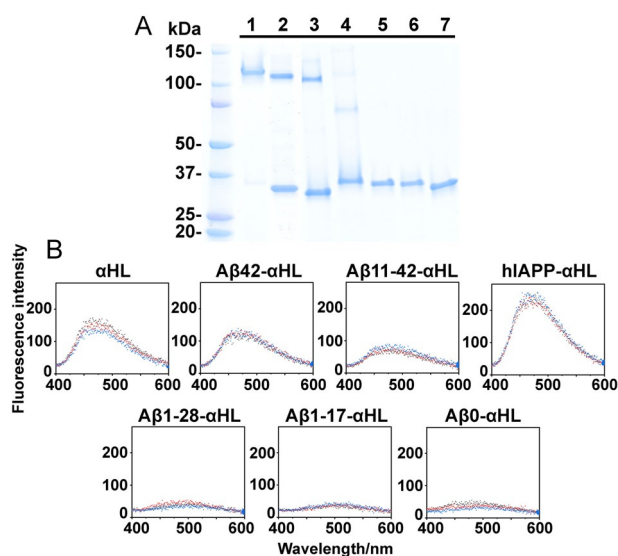
Figure 2. A) Purification of WT αHL and hybrid amyloid-αHL oligomers with a Co-NTA column in 50 mM Tris-HCl, pH 8.0 with 0.5 M NaCl, 250 mM imidazole and 0.38 mM DDM micelles. Lane 1: WT αHL; lane 2–3: hybrid Aβ42-αHL and Aβ11-42-αHL; lane 4: hybrid hIAPP-αHL; lane 5–7: hybrid Aβ1-28-αHL, Aβ1-17-αHL and Aβ0-αHL, respectively. SDS-PAGE electrophoresis was conducted at 200 V for 25 min. B) Fluorescence emission spectra of 20 μM ANS binding to 10 μM WT αHL or hybrid amyloid-αHL oligomers at excitation wavelength 350 nm. The fluorescence was recorded at wavelengths from 400–600 nm at room temperature in 50 mM Tris-HCl, pH 8.0 with 0.5 M NaCl, 250 mM imidazole and 0.38 mM DDM micelles. Each experiment was repeated three times independently.
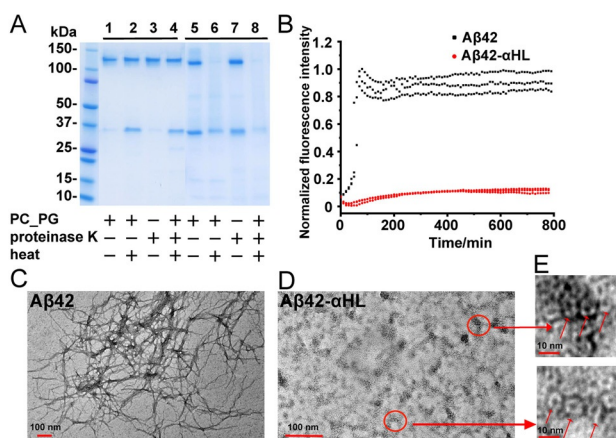
Figure 3. A) Limited proteolysis with proteinase K of the WT αHL and hybrid Aβ42-αHL oligomers in the presence of DOPC:DOPG (4:1) liposomes (1 mg mL⁻¹). Lane 1: αHL treated with DOPC:DOPG liposomes; lane 2: αHL oligomers treated with DOPC:DOPG liposomes and then heat denatured at 95 °C for 15 min; lane 3: αHL oligomers digested with proteinase K; lane 4: αHL oligomers treated with DOPC:DOPG liposomes was further digested by proteinase K and then heat-denatured at 95 °C. Lane 5–8 had the same conditions as 1–4, but hybrid Aβ42-αHL oligomers were used. B) ThT measurement of fibril formation of WT Aβ42 and hybrid Aβ42-αHL in 50 mM Tris-HCl, pH 8.0 with 0.5 M NaCl, 250 mM imidazole and 0.38 mM DDM. The ratio of ThT and the peptides was 4:1 with a ThT final concentration 40 μM. The excitation and emission filters were 430 and 480 nm, respectively. C–E) TEM images of WT Aβ42 fibrils and hybrid Aβ42-αHL proteins, after the fibrillation kinetics of these samples analyzed by the ThT-assay. Scale bars of Aβ42 fibrils and hybrid Aβ42-αHL oligomers are 100 nm. The zoom-in scale bar is 10 nm.

fluorescence spectroscopy.[18] At the same concentration, αHL, Aβ42-αHL, Aβ11-42-αHL and hIAPP-αHL all form oligomers with more hydrophobic surfaces for ANS binding (Figure 2 B). These results indicate that the amyloid sequence drives oligomerization whilst the αHL scaffold determines the stoichiometry.

The oligomers of WT αHL remain stable after proteinase K treatment (Figure 3 A, lane 3), while αHL monomers begin to degrade (Figure S4), as reported previously.[19] This indicates that the assembly state of αHL determines the proteolysis-resistance. However, both the monomeric and heptameric Aβ42 on the αHL scaffold are resistant to proteolysis (Figure 3 A, lane 7&8). This is in agreement with previous studies showing that WT Aβ42 monomers and oligomers are resistant to proteolysis.[20] Apparently, Aβ42 can retain this property on the αHL scaffold. However, hybrid Aβ11-42-αHL and hIAPP-αHL monomers as well as the oligomers can be proteolyzed (Figure S4), suggesting that the Aβ11-42 and hIAPP oligomers are less stable than the Aβ42 oligomers on the scaffold. Aβ1-28-αHL and Aβ1-17-αHL (Figure S5) monomers are also proteolyzed, revealing that the amyloid sequence dominates the stability and protease resistance of the displayed oligomers.

After heat denaturation of αHL (Figure 3 A, lane 2&4), we observed more monomeric αHL, indicating dissociation of the oligomers. However, hybrid Aβ42-αHL (Figure 3 A, lane 6&8) and Aβ11-42-αHL (Figure S4) are lost upon heat

treatment, probably due to aggregation or precipitation. This indicates these constructs can assemble into aggregates larger than heptamers. It has been observed in several studies that, compared to neutrally charged lipids, negatively charged lipid bilayers have stronger interactions with amyloid peptides such as Aβ,[21] α-synuclein[22] and Tau.[23] In order to determine the effect of lipid charge on hybrid sequence oligomerization, we incubated these hybrid oligomers with a mixture of DOPC:DOPG (4:1). The Aβ42 sequence exhibits similar oligomerization properties in the presence of neutrally charged DPhPC liposomes (Figure S5), suggesting that the charge of the lipid membranes does not modulate Aβ42-αHL oligomerization. But we cannot exclude that the charge may influence the flexibility of local structure or fibrillation.

ThT fluorescence monitors amyloid formation.[24] ThT fluorescence of WT Aβ42 in the presence of 0.38 mM DDM increases much more than that of Aβ42-αHL (Figure 3 B), indicating that the Aβ42 fibril formation is inhibited on the αHL. TEM confirmed that hybrid Aβ42-αHL remains present as stable heptameric pores, even after incubation in the ThT assay (Figure 3 D&E). The small increase of the ThT fluorescence signal in the presence of hybrid Aβ42-αHL could have been caused by the formation of the observed oligomers or amorphous aggregates, and not by fibrils, which we did not observe in the TEM images (Figure 3 E&S6H). As shown in Figure 3 B, WT Aβ42 fibril formation can be observed at around 100 min in the presence of DDM micelles, and is delayed to 500 min without DDM (Figure S6A). Hybrid hIAPP-αHL also gives much less ThT fluorescence than WT hIAPP with or without DDM micelles (Figure S6D–S6F). ThT assays confirmed that WT αHL does not form fibrils (Figure S6C) and remains present as a stable pore, as indicated by TEM imaging (Figure S6G). The slightly different ThT results of WT αHL and the hybrid Aβ42-αHL may reflect a different binding of ThT to the β-barrel, which could be indicative of the different barrel quaternary structures. The low fluorescence values in the presence of Aβ11-42-αHL, Aβ1-28-αHL, Aβ1-17-αHL or Aβ0-αHL (Figure S6B) reveal that the αHL scaffold does not interfere with the ThT fluorescence assay. These results confirm that the αHL scaffold confines the displayed Aβ42 oligomers and prevents their fibrillation into amyloid.

The interaction of WT Aβ42/Aβ42-αHL/αHL oligomers with lipid bilayers was studied using single-channel electrical recordings. WT Aβ42 and Aβ42-αHL oligomers form channels with similar conductance (I/V), which varies from 0.2 to 0.5 nS (Figure 4). The variation and fluctuation of the current is likely caused by the dynamics and heterogeneity of the oligomers, which was also reported by others.[4b,c] Aβ42-αHL oligomers apparently retain the characteristic of Aβ42-pores. This indicates that the amyloid sequence is not only required for the oligomerization of Aβ42-αHL sequence but also determines the channel flexibility of the oligomer in lipid membranes. Both Aβ42-αHL and WT Aβ42 channels appear to be smaller and more dynamic than the WT αHL channel which has a conductance of 0.8 nS. The discrepancy between the WT αHL and Aβ42-αHL channels further confirmed that the transmembrane sequence plays a very important role in determining the size and flexibility of the channels in lipid
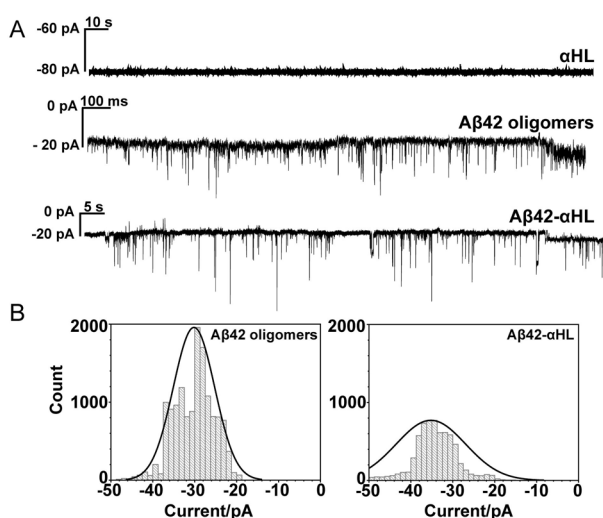
Figure 4. A) Representative current traces of pore formation by WT αHL, Aβ42 oligomers, and hybrid Aβ42-αHL oligomers in the DOPC:-DOPG (4:1) lipid bilayers. Currents were measured in 1 M KCl, 10 mM Hepes (pH 7.4) under −100 mV at room temperature. Aβ42 oligomers were measured in the presence of 0.38 mM DDM micelles. B) Histograms of the counts generated by the current traces of Aβ42 oligomers and hybrid Aβ42-αHL oligomers. Solid curves were obtained by fitting a Gaussian.

membranes. The spread of measured current is higher in the case of pore formation by WT Aβ42 oligomers, compared to Aβ42-αHL oligomers (Figure 4). This could be caused by the non-uniform stoichiometry of the WT pores, compared to the heptameric Aβ42-αHL pores, leading to a predictable increased variability of pore diameters.

As the pores formed by WT αHL and Aβ42-αHL show clear differences, they may also differ in cell toxicity. A hemolytic assay (Figure 5A), showed that both Aβ42-αHL and WT Aβ42 oligomers are less hemolytic than WT αHL (which has a HC50 of 24 ngmL^{-1}, the concentration of protein giving 50% lysis at 120 min, $n=3$). Truncated αHL also has very weak hemolytic activity,[25] indicating that Aβ42-αHL and Aβ42 oligomers hardly penetrate erythrocyte membranes. Additionally, we found that WT Aβ42, Aβ42-αHL and Aβ11-42-αHL oligomers behave similarly in the neuronal toxicity assays (Figure 5C). This indicates that the αHL scaffold does not interfere to a major extent with the toxicity of WT Aβ oligomers. WT αHL is the most toxic for the neuroblastoma cells, which is in line with the single-channel electrical recordings indicating that WT αHL has much higher conductance (around 0.8 nS) than WT Aβ42 (0.2–0.5 nS).

A conformation-specific amyloid oligomer antibody, A11, was used to confirm the structural similarity between the Aβ42-αH oligomers and WT Aβ42 oligomers (Figure 5B&S7). We observed that αHL (lane 1), Aβ42-αHL (lane 2), Aβ11-42-αHL (lane 3), hIAPP-αHL (lane 4) and WT Aβ42 oligomers (lane 5) can all bind the A11 antibody. Strikingly, the αHL oligomers show the clearest signal, suggesting that the β-barrel moiety of αHL-displayed Aβ oligomers adopts a wider range of conformations and remains more flexible than WT αHL's, which is also suggested by our
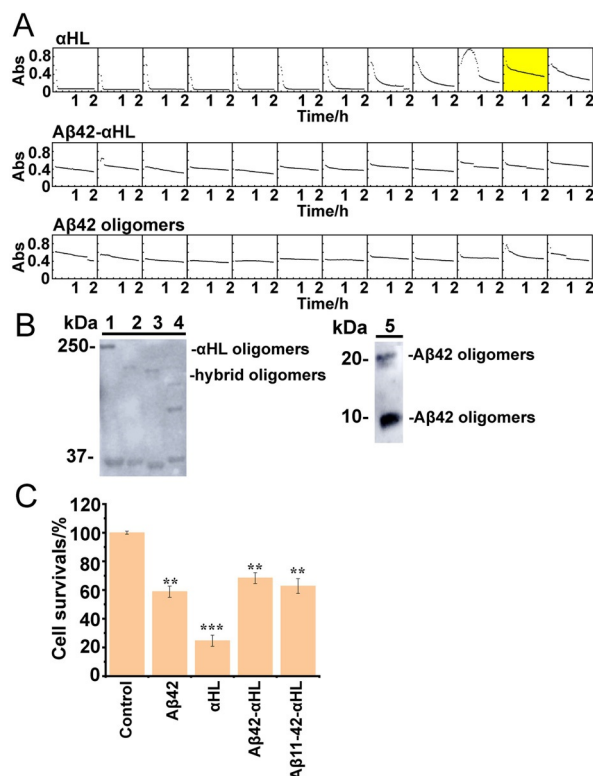
Figure 5. A) Hemolysis by WT αHL oligomers, hybrid Aβ42-αHL or WT Aβ42 oligomers oligomers. The HC50 of WT αHL (50% cell lysis in 120 min at 37 °C; yellow box) is 24 ng mL^{-1}, indicating specific hemolytic activity. The decrease of absorbance (Abs, y-axis, from 0–1) in light scattering over time (x-axis) was recorded in a microplate reader at 595 nm for 2 h at room temperature. B) Immunogenic similarity of WT αHL, hybrid Aβ42/11–42-αHL and Aβ42 oligomers by western blot. The anti-Aβ42 oligomer conformation-dependent antibody A11 recognized αHL oligomers (lane 1); hybrid Aβ42-αHL oligomers (lane 2); hybrid Aβ11-42-αHL oligomers (lane 3); hybrid hIAPP-αHL oligomers (lane 4) and Aβ42 oligomers (lane 5). The SDS-PAGE electrophoresis prior to blotting, was conducted at 120 V for 80 min. C) SH-SY5Y cell viability using a luminescence assay (error bars determined by triplicate experiments). 5 μM WT αHL, Aβ42 and hybrid Aβ42-αHL oligomers were treated with SH-SY5Y cells with 6000 cells/well density after incubating for 48 h at 37 °C, 5% CO$_2$. The results are shown as percentages of control samples. All the Aβ42 oligomers were prepared in the presence of 0.38 mM DDM micelles. Data are represented as the mean S.E.M (standard error of the mean). Two-tailed student's t-test was applied for statistical significance. **$P<0.01$ (very significant) and ***$P<0.001$ (highly significant) were compared to the control.

single particle cryo-EM analysis. These cellular and functional assays suggest that Aβ42-αHL and Aβ42 oligomers share functional and toxicological properties, with a lower toxicity to neuronal and red blood cells compared to αHL.

To determine the 3D structure of the Aβ42 oligomer as stabilized by the αHL scaffold, more than 4000 cryo-EM movies of Aβ42-αHL were collected under cryogenic conditions on a Titan Krios. Two representative regions with a high amount of Aβ42-αHL particles are shown in Figure S11. Some particle projection averages (Figure S12, not framed in the red box) are excluded due to the noise or contamination. We found the cryo-EM sample to be very
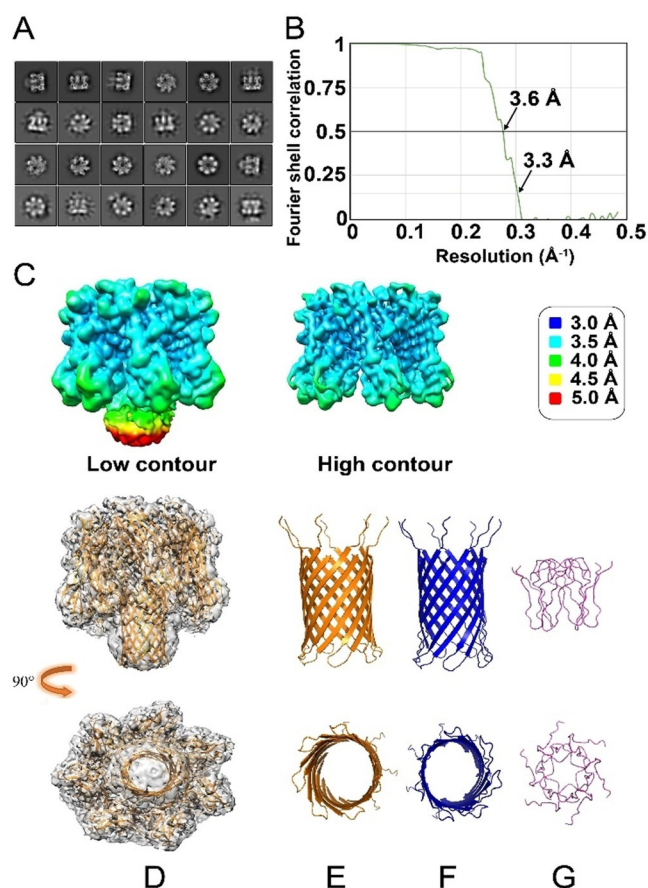
Figure 6. Cryo-EM data of Aβ42-αHL. A) 2D classes show strong features for the αHL heptameric core, along with clear but more diffuse density for the structure formed by the Aβ42 sequences. B) The 3D average after the classification and refinement has an overall resolution of 3.3 Å at FSC = 0.143 calculated by the gold-standard Fourier shell correlation (3.6 Å at FSC = 0.5). C) The local resolution density map of hybrid Aβ42-αHL (left) and the αHL scaffold at a higher contour (right). The resolution is color-coded according to the legend on the right. The lower local resolution of the Aβ42 pore region (Low contour, mainly the yellow and red colors), compared to the better local resolution of the αHL part (High contour, mainly the blue and cyan colors) indicates structural flexibility and/or heterogeneity for the pore region. D) Side (upper image) and top (lower image) views of molecular representation of heptameric Aβ42-αHL in the electron density map (PDB ID: 7O1Q, EMD-12696). E–G) The comparison of the structures from the side and top views. αHL-displayed Aβ42 pore (yellow, E); WT αHL transmembrane pore (blue, F) and hexameric Aβ42cc (residues 15–42, light purple, G) built by NMR restrained Rosetta simulation with the smallest pore diameter.[26]

homogeneous and no other classes are identified of oligomers other than heptamers. Some 2D classes showing strong features for αHL heptameric core are shown in Figure 6A. 141′366 particles were averaged to a final overall resolution of 3.3 Å (Figure 6B&Table 1). The 3D map shows high-resolution density for the symmetrical core of the αHL scaffold (Figure 6C, EMD-12696). However, the density in the Aβ42 region is weaker and more diffuse, indicative of its flexible nature.

Absence of atomically resolved density for the Aβ42 region prompts us to investigate several possible pairings

Table 1: Cryo-EM structure determination.

Data collection	
Magnification	48′540×
Pixel size [Å]	1.03
Defocus Range [μm]	−0.9 to −3.0
Voltage [kV]	300
Exposure time [s per frame)	0.2
Number of frames	50
Total dose [eÅ⁻²]	55
Reconstitution	
Box size [pixels]	200
Symmetry	C7
Micrographs	4′284
Automatically picked particles	2′438′446
Particles after 2D classification	204′103
Particles after 3D classification	141′366
Resolution after 3D auto-refine [Å]	3.5
Final overall resolution [Å]	3.3
Estimated map sharpening B-factor [Å²]	−124.06

between adjacent Aβ42 β-hairpins within the membrane-crossing β-barrel. These quaternary structural pairings are compared on the basis of their energies, as calculated by the Rosetta software (Figure S8). On the basis of this analysis, we propose a pairing that also fits best into the density (Figure S8), and the atomic structure (PDB ID: 7O1Q) from the refinement (Table S2) is presented in Figure 6D&E. A superposition of this most likely model with WT αHL electron density is shown in Figure S9. The apparent dome shape of hybrid Aβ42-αHL barrel is most likely an artifact of the cryo-EM reconstruction of the flexible Aβ region caused by the application of C7 symmetry. The dynamic conformation of Aβ42 region may explain why Aβ42-αHL forms a fluctuating, transient pore, that we observed by the single-channel electrical recordings. The molecular reconstruction of the Aβ42 oligomer in the electron density map of the hybrid Aβ42-αHL, shows it is a bit shorter (Figure 6E, Figure S8&S9) than that of WT αHL (Figure 6F). The superposition of Aβ42-αHL and WT αHL oligomers shows slightly different β-hairpin topologies in the β-barrels (Figure S10). But the Rosetta energy of WT αHL's β-barrel is much lower than that of Aβ42-αHL in Figure S8. This implies that the β-barrel conformational change is closely associated with its energy, presumably modulating the interaction with lipid membranes. These structures and energy characteristics are in line with the observed functional and electrophysiological behavior of the Aβ42-αHL, compared to WT αHL.

In the "toxic Aβ oligomer" hypothesis,[27] the Aβ peptides assemble into diverse β-barrel oligomers that breach the integrity of cellular membranes, thus compromising cell viability. The structural and functional characterization of transient and stoichiometric heterogeneous Aβ oligomers is challenging in lipid bilayers, though Aβ oligomers can be stabilized by protein engineering[28] and photo-induced cross-linking.[29] By replacing the transmembrane β-hairpin of αHL by Aβ42, we are able to assemble Aβ42 into stable heptamers, structurally and functionally similar to the wild-type oligomers, yielding a single, unique oligomer species for single-

particle cryo-EM analysis, biophysical characterization and functional studies.

Our data show that the Aβ sequence is required for oligomerizing the αHL scaffold. Deletion of parts of the Aβ-sequence abrogates oligomerization of the αHL moiety: neither the hybrid Aβ1-17 or 1–28-αHL proteins, nor the control Aβ0-αHL lacking all β-hairpin sequences oligomerizes in a lipid-mimicking environment. This observation is consistent with the principle that the C-terminus of Aβ modulates Aβ oligomerization.[30] These data also confirm our hypothesis that its amyloid sequence retains its oligomerizing properties when displayed on the αHL scaffold. The resistance to proteolysis and fibrillation confirms the conformational stability of the Aβ42-αHL oligomers. Single-channel electrical recordings reveal that both Aβ42-αHL oligomers and WT Aβ42 oligomers exhibit typical open channel characteristics (approximately 0.2–0.5 nS conductance) with frequent spikes, in line with similar studies on Aβ42 oligomers.[31] The "spiky" behavior of the current is most likely caused by the dynamics of Aβ42 within the negatively charged membranes.[32] Single-particle cryo-EM analysis confirms that the conformational flexibility that characterized Aβ42 oligomers is retained within the Aβ42-αHL oligomers too. These results suggest that Aβ42-αHL and the WT oligomers similarly interact with lipid bilayers.

Our cellular assays (Figure 5 A&C) and western blots (Figure 5 B) further confirm the structurally similarities between Aβ42-αHL and WT Aβ42 oligomers. Both have negligible hemolytic activity towards rabbit erythrocytes, unlike WT αHL oligomers (hemolytic activity HC50 = 24 ng mL^{-1}), suggesting that the erythrocyte membrane is penetrated by Aβ42 oligomers to a much lesser extent. This is consistent with the weak or lost hemolytic activity of truncated αHL.[25] WT αHL oligomers also have the highest toxicity to SH-SY5Y neuroblastoma cells, compared to Aβ42-αHL and WT Aβ42 oligomers, in line with our single-channel electrical recordings and hemolytic assays. These results indicate that the heptamers of WT αHL form larger inner-diameter channels than Aβ42-αHL. Olson et al. suggested the pre-stem of αHL converts its conformation, prior to the insertion of the β-strands into the membranes.[33] It is highly plausible that Aβ42 oligomerizes on the displayed scaffold followed by the insertion into lipid bilayers. The β-barrel length of WT αHL or Aβ oligomers may play an important role in their toxicity.

The αHL scaffold can also accommodate other amyloid pore-forming sequences, as we demonstrate with the hIAPP-αHL hybrid. The outer-membrane αHL moiety not only increases the size of the pore-forming oligomers, which improves the resolution in cryo-EM imaging, but also prevents fibril formation. Our cryo-EM reconstruction shows the scaffold of αHL at a resolution of 3.3 Å, but the resolution of the Aβ42 region is lower (4 to 5 Å). Our best structural model (shown in Figure 6 D and Figure S9) suggests that the Aβ42 β-barrel pore has a shorter length (35.5 Å) and a similar inner diameter (27.4 Å) of the largest circular cross-section, compared to the WT αHL barrel (47.8 Å high and 23.8 Å wide[9]). It is longer than a truncated hexameric β-barrel model of Aβ (residues 15–42) built by NMR restrained

Rosetta simulation.[26] We compared all these structures in Figure 6 E–G. The observation of a shorter transmembrane length of Aβ42-αHL compared to WT αHL is consistent with our single-channel electrical recordings. We propose that the relatively short transmembrane pore length of the displayed Aβ oligomers affects its interaction with lipid bilayers, which may explain its reduced cell toxicity compared to pores with longer transmembrane domains, like WT αHL.

Stabilizing physiologically relevant, toxic Aβ oligomers allows structure determination and contributes to our understanding of amyloid toxicity in AD. The Nuttall lab determined non-toxic Aβ18-41 dimer/tetramer on an antigen receptor.[34] That hybrid Aβ18-41 does not show a β-turn-β hairpin structure as observed in other studies.[6c,26] In addition, the Aβ18-41 oligomer that is buried in the scaffold, is more difficult to functionally compare with the WT Aβ, as it can't form a pore or insert into a lipid membrane. Sandberg et al. engineered a double-cysteine Aβ42 mutant to stabilize Aβ oligomers with β-sheet conformation.[28] The stabilized Aβ42 oligomers in the absence of lipid membranes, mainly a mixture of dimers and trimers, are prone to form protofibrils.

WT Aβ42 oligomers likely form heterogeneous structures in the presence of cellular membranes. Our alternative method enables generating functionally and structurally relevant oligomers, displayed as heptameric pores in membrane mimicking DDM micelles. Similar heterogenic pore forming Aβ oligomers were observed in the presence of DDM micelles.[6a] Österlund et al. concluded from native mass spectrometry that the β-barrel pore-forming hexamer might be the biggest Aβ oligomer in the presence of DDM micelles.[6b] However, hexameric oligomers would result in a significantly narrower pore than we observed for the Aβ42-αHL heptamers (Figure 6 G), which would not be in line with the single pore conductance results we report here (Figure 4 A). Possibly, the native mass spectroscopy is insensitive to higher molecular-weight oligomers that were reported in other studies,[35] or DDM micelles preferentially incorporate hexameric oligomers. We point out potential disadvantages of our design: (1) the buried N-terminal or C-terminal Aβ peptides in the scaffold will be not available for antibody targeting;[36] (2) the moiety of αHL only allows Aβ to aggregate into one species of heptameric oligomer for structural and functional characterization, and no other oligomeric states.

Conclusion

We propose a novel protein scaffold for generating a single Aβ42 oligomer species for biochemical characterization and structure determination. We anticipate that the hybrid construct may help to enhance our understanding of the structure and dynamics of amyloid oligomers in lipid membranes, yielding novel insights into the molecular mechanism of oligomer toxicity. Our results also contribute to understanding membrane protein oligomerization in lipid membranes, especially with regard to the β-sheet-containing proteins that appear to form polymorphic ion channels. Further, the αHL-displayed oligomers, as a mimetic antigen, with a well-defined

stoichiometry, may allow developing novel, conformation-specific antibodies. This would allow alternative approaches for developing immuno-based diagnostics and potentially even therapies for AD and other neurodegenerative diseases.

Conflict of interest

The authors declare no conflict of interest.

Keywords: Aβ42 oligomer · electron microscopy · protein structures · α-hemolysin

[1] C. A. Ross, M. A. Poirier, *Nat. Med.* **2004**, *10 Suppl*, S10–17.

[2] J. Hardy, D. J. Selkoe, *Science* **2002**, *297*, 353–356.

[3] H. A. Lashuel, D. Hartley, B. M. Petre, T. Walz, P. T. Lansbury, *Nature* **2002**, *418*, 291-2-91.

[4] a) N. Arispe, H. B. Pollard, E. Rojas, *Proc. Natl. Acad. Sci. USA* **1993**, *90*, 10573–10577; b) A. Quist, I. Doudevski, H. Lin, R. Azimova, D. Ng, B. Frangione, B. Kagan, J. Ghiso, R. Lal, *Proc. Natl. Acad. Sci. USA* **2005**, *102*, 10427–10432; c) H. Jang, F. T. Arce, S. Ramachandran, R. Capone, R. Azimova, B. L. Kagan, R. Nussinov, R. Lal, *Proc. Natl. Acad. Sci. USA* **2010**, *107*, 6538–6543.

[5] A. Demuro, M. Smith, I. Parker, *J. Cell Biol.* **2011**, *195*, 515–524.

[6] a) M. Serra-Batiste, M. Ninot-Pedrosa, M. Bayoumi, M. Gairí, G. Maglia, N. Carulla, *Proc. Natl. Acad. Sci. USA* **2016**, *113*, 10866–10871; b) N. Österlund, R. Moons, L. L. Ilag, F. Sobott, A. Gräslund, *J. Am. Chem. Soc.* **2019**, *141*, 10440–10450; c) S. Ciudad, E. Puig, T. Botzanowski, M. Meigooni, A. S. Arango, J. Do, M. Mayzel, M. Bayoumi, S. Chaignepain, G. Maglia, S. Cianferani, V. Orekhov, E. Tajkhorshid, B. Bardiaux, N. Carulla, *Nat. Commun.* **2020**, *11*, 3014.

[7] a) S. M. Butterfield, H. A. Lashuel, *Angew. Chem. Int. Ed.* **2010**, *49*, 5628–5654; b) J. Wu, C. Cao, R. A. Loch, A. Tiiman, J. Luo, *Q. Rev. Biophys.* **2020**, *53*, e12; c) R. Kayed, Y. Sokolov, B. Edmonds, T. M. McIntire, S. C. Milton, J. E. Hall, C. G. Glabe, *J. Biol. Chem.* **2004**, *279*, 46363–46366.

[8] R. Henderson, *Q. Rev. Biophys.* **1995**, *28*, 171–193.

[9] L. Song, M. R. Hobaugh, C. Shustak, S. Cheley, H. Bayley, J. E. Gouaux, *Science* **1996**, *274*, 1859–1866.

[10] Y. Yoshiike, R. Kayed, S. C. Milton, A. Takashima, C. G. Glabe, *NeuroMol. Med.* **2007**, *9*, 270–275.

[11] Y. Du, L. Liu, C. Zhang, Y. Zhang, *Infect. Drug Resist.* **2018**, *11*, 1271–1274.

[12] W. Hoyer, C. Grönwall, A. Jonsson, S. Ståhl, T. Härd, *Proc. Natl. Acad. Sci. USA* **2008**, *105*, 5099–5104.

[13] T. Lührs, C. Ritter, M. Adrian, D. Riek-Loher, B. Bohrmann, H. Döbeli, D. Schubert, R. Riek, *Proc. Natl. Acad. Sci. USA* **2005**, *102*, 17342–17347.

[14] T. Kawate, E. Gouaux, *Protein Sci.* **2003**, *12*, 997–1006.

[15] E. T. A. S. Jaikaran, A. Clark, *Biochim. Biophys. Acta Mol. Basis Dis.* **2001**, *1537*, 179–203.

[16] C. Poojari, D. Xiao, V. S. Batista, B. Strodel, *Biophys. J.* **2013**, *105*, 2323–2332.

[17] C. Peters, D. Bascuñán, C. Opazo, L. G. Aguayo, *J. Alzheimer's Dis.* **2016**, *51*, 689–699.

[18] B. Bolognesi, J. R. Kumita, T. P. Barros, E. K. Esbjorner, L. M. Luheshi, D. C. Crowther, M. R. Wilson, C. M. Dobson, G. Favrin, J. J. Yerbury, *ACS Chem. Biol.* **2010**, *5*, 735–740.

[19] L. Jayasinghe, G. Miles, H. Bayley, *J. Biol. Chem.* **2006**, *281*, 2195–2204.

[20] a) L. O. Tjernberg, J. Näslund, J. Thyberg, S. E. Gandy, L. Terenius, C. Nordstedt, *J. Biol. Chem.* **1997**, *272*, 1870–1875; b) F. Langer, Y. S. Eisele, S. K. Fritschi, M. Staufenbiel, L. C. Walker, M. Jucker, *J. Neurosci.* **2011**, *31*, 14488–14495; c) A. Ruiz-Riquelme, H. H. C. Lau, E. Stuart, A. N. Goczi, Z. Wang, G. Schmitt-Ulms, J. C. Watts, *Acta Neuropathol. Commun.* **2018**, *6*, 26.

[21] a) X. Yu, Q. Wang, Q. Pan, F. Zhou, J. Zheng, *Phys. Chem. Chem. Phys.* **2013**, *15*, 8878–8889; b) H. Ahyayauch, M. Raab, J. V. Busto, N. Andraka, J.-L. R. Arrondo, M. Masserini, I. Tvaroska, F. M. Goñi, *Biophys. J.* **2012**, *103*, 453–463.

[22] a) W. S. Davidson, A. Jonas, D. F. Clayton, J. M. George, *J. Biol. Chem.* **1998**, *273*, 9443–9449; b) K. Pirc, N. P. Ulrih, *Biochim. Biophys. Acta Biomembr.* **2015**, *1848*, 2002–2012; c) B. D. van Rooijen, M. M. A. E. Claessens, V. Subramaniam, *Biochim. Biophys. Acta Biomembr.* **2009**, *1788*, 1271–1278.

[23] E. M. Jones, M. Dubey, P. J. Camp, B. C. Vernon, J. Biernat, E. Mandelkow, J. Majewski, E. Y. Chi, *Biochemistry* **2012**, *51*, 2539–2550.

[24] R. Khurana, C. Coleman, C. Ionescu-Zanetti, S. A. Carter, V. Krishna, R. K. Grover, R. Roy, S. Singh, *J. Struct. Biol.* **2005**, *151*, 229–238.

[25] D. Stoddart, M. Ayub, L. Höfler, P. Raychaudhuri, J. W. Klingelhoefer, G. Maglia, A. Heron, H. Bayley, *Proc. Natl. Acad. Sci. USA* **2014**, *111*, 2425–2430.

[26] C. Lendel, M. Bjerring, A. Dubnovitsky, R. T. Kelly, A. Filippov, O. N. Antzutkin, N. C. Nielsen, T. Härd, *Angew. Chem. Int. Ed.* **2014**, *53*, 12756–12760.

[27] E. N. Cline, M. A. Bicca, K. L. Viola, W. L. Klein, *J. Alzheimer's Dis.* **2018**, *64*, S567–S610.

[28] A. Sandberg, L. M. Luheshi, S. Söllvander, T. Pereira de Barros, B. Macao, T. P. Knowles, H. Biverstål, C. Lendel, F. Ekholm-Petterson, A. Dubnovitsky, L. Lannfelt, C. M. Dobson, T. Härd, *Proc. Natl. Acad. Sci. USA* **2010**, *107*, 15595–15600.

[29] G. Bitan, M. D. Kirkitadze, A. Lomakin, S. S. Vollers, G. B. Benedek, D. B. Teplow, *Proc. Natl. Acad. Sci. USA* **2003**, *100*, 330–335.

[30] a) E. A. Fradinger, B. H. Monien, B. Urbanc, A. Lomakin, M. Tan, H. Li, S. M. Spring, M. M. Condron, L. Cruz, C. W. Xie, G. B. Benedek, G. Bitan, *Proc. Natl. Acad. Sci. USA* **2008**, *105*, 14175–14180; b) L. M. Gordon, A. Nisthal, A. B. Lee, S. Eskandari, P. Ruchala, C. L. Jung, A. J. Waring, P. W. Mobley, *Biochim. Biophys. Acta* **2008**, *1778*, 2127–2137.

[31] N. Arispe, H. B. Pollard, E. Rojas, *Proc. Natl. Acad. Sci. USA* **1996**, *93*, 1710–1715.

[32] M. Grimaldi, M. Scrima, C. Esposito, G. Vitiello, A. Ramunno, V. Limongelli, G. D'Errico, E. Novellino, A. M. D'Ursi, *Biochim. Biophys. Acta* **2010**, *1798*, 660–671.

[33] R. Olson, H. Nariya, K. Yokota, Y. Kamio, E. Gouaux, *Nat. Struct. Biol.* **1999**, *6*, 134–140.

[34] V. A. Streltsov, J. N. Varghese, C. L. Masters, S. D. Nuttall, *J. Neurosci.* **2011**, *31*, 1419–1426.

[35] a) N. Kandel, T. Zheng, Q. Huo, S. A. Tatulian, *J. Phys. Chem. B* **2017**, *121*, 10293–10305; b) N. Kandel, J. O. Matos, S. A. Tatulian, *Sci. Rep.* **2019**, *9*, 2689.

[36] D. Frenkel, M. Balass, E. Katchalski-Katzir, B. Solomon, *J. Neuroimmunol.* **1999**, *95*, 136–142.